Beam Properties of Visible Proton-Implanted Photonic Crystal VCSELs

Ansas M. Kasten, *Student Member, IEEE*, Dominic F. Siriani, *Student Member, IEEE*, Mary K. Hibbs-Brenner, *Member, IEEE*, Klein L. Johnson, and Kent D. Choquette, *Fellow, IEEE*

(Invited Paper)

***Abstract*—We investigate the optical properties of proton-implanted photonic crystal (PhC) vertical-cavity surface-emitting lasers (VCSELs) emitting in the visible spectrum. The fabricated lasers have a threshold current of 1.3 mA and single-mode output power greater than 1 mW at room temperature. The incorporation of a PhC into the top facet of a proton-implanted VCSEL results in a stable single-fundamental-mode operation with a side-mode suppression ratio larger than 30 dB and a constant beam divergence independent of injection current level or ambient temperature. Using an index-step optical fiber model, we compare the effects of different hole etching depths to variations in output beam divergence. By varying the design and etching depth of the hole pattern, the lasers can either be optimized for low beam divergence or low threshold currents. The controllable refractive index guidance effect from the PhC allows for precise engineering of the optical properties of these visible VCSELs for consumer and imaging applications.**

***Index Terms*—High-quality beam properties, imaging applications, proton-implanted photonic crystal (PhC), single-mode operation, vertical-cavity surface-emitting laser (VCSEL), visible semiconductor lasers.**

I. Introduction

VERTICAL-CAVITY surface-emitting lasers (VCSELs) have advantages over other semiconductor lasers due to their inherent characteristics of surface emission, circular optical output beam, low power operation, ease of integration in 2-D arrays, and low-cost/high-volume manufacture. Consequently, VCSELs have been the light source of choice in a variety of optoelectronic applications such as free-space optical interconnects [1], short haul data transmission [2], optical data storage [3], and optical sensing [4], [5]. In particular, red VCSELs, with their high-speed modulation capabilities, are a preferred light source for plastic optical fiber (POF) data transmission [6]–[8] due to the attenuation minimum of the POF in the 650-nm range. Furthermore, VCSELs emitting in the visible spectrum are interesting candidates for various sensing and display applications. Most of these applications demand a high-quality single-mode output beam. A narrow and stable beam divergence is beneficial for accurate position sensing, high fiber coupling efficiency, homogeneous illumination of displays, and projection of sharp images.

Despite many positive characteristics, conventional VCSELs also have disadvantages, especially, in terms of single-fundamental-mode operation. Due to their large diameter or large refractive index lateral confinement, generic VCSELs typically operate in multiple transverse modes. Several transverse optical confinement approaches have been investigated to achieve a single-fundamental-mode operation including small oxide apertures [9], small implant apertures [10], hybrid oxide/implant structures [11], surface relief etched lasers [12], [13], etched holy pattern [14], [15], and photonic crystal (PhC) lasers [16]–[22]. All these approaches favor the single-fundamental-mode operation by either increasing the gain for the fundamental mode, increasing the loss of higher order modes, or by engineering the transverse index profile of the VCSEL to support only the lowest order mode. In this paper, we focus on an index-guided single-mode PhC VCSELs emitting in the visible range of the optical spectrum.

Previous works have shown excellent performance for proton-implanted and oxide-confined InGaAlP-based VCSELs emitting in the 640–690-nm wavelength region [23]–[28]. Due to the strong optical and electrical confinement provided by the oxide layer, oxide-confined VCSELs typically show superior device characteristics and demonstrate higher output powers, lower threshold currents, and improved internal quantum efficiency compared to the proton-implanted counterpart [29]–[31]. However, it is the same strong index guiding effect of the oxide layer that makes the single-fundamental-mode operation more difficult to achieve. As a result, conventional oxide-confined VCSELs require a small oxide aperture to operate in a single fundamental mode [32]. This limits the maximum achievable output power as well as reduces the device reliability due to high current densities in the oxide-confined region.

In contrast, proton-implanted VCSELs inherently operate in the single fundamental mode for low levels of current injection

Manuscript received December 1, 2010; revised February 16, 2011; accepted February 22, 2011. Date of publication April 25, 2011; date of current version December 7, 2011. This work was supported in part by the Nano-Chemical-Electrical-Mechanical Manufacturing Systems (CEMMS), University of Illinois's Nano-Science and Engineering Center (NSEC) and in part by the National Science Foundation (NSF) under Award DMI 0328162.

A. M. Kasten, D. F. Siriani, and K. D. Choquette are with the Electrical and Computer Engineering Department, University of Illinois at Urbana-Champaign, Urbana, IL 61801 USA (e-mail: akasten@illinois.edu; siriani@illinois.edu; choquett@illinois.edu).

M. K. Hibbs-Brenner and K. Johnson are with Vixar Corporation, Plymouth, MN 55447 USA (e-mail: mhibbsbrenner@vixarinc.com; kjohnson@vixarinc.com).

Color versions of one or more of the figures in this paper are available online at http://ieeexplore.ieee.org.

Digital Object Identifier 10.1109/JSTQE.2011.2125780

due to the weak index confinement provided by the thermal lens. However, for higher levels of current injection or varying ambient temperatures, multimode operation, random beam steering, and, consequently, an increase in far-field divergence are observed. The stability of the output beam of proton-implanted VCSELs is especially problematic under pulsed operation due to the lack of the thermal lens. A PhC with a single defect in the center region etched into the top facet of a proton-implanted VCSEL solves these problems and allows for a stable high-quality single-fundamental-mode output beam for all levels of current injection and varying ambient temperatures. In proton-implanted PhC VCSELs, the optical confinement is determined by the PhC pattern whereas the electrical confinement is provided by the proton-implant aperture.This allows for precise engineering of the index guidance effect of the PhC without altering the electrical confinement of the VCSEL. The index step of the PhC defect cavity can be engineered by carefully designing the periodic hole pattern as well as by controlling the etching depth of the air holes [33]. However, to simply achieve single-fundamental-mode operation, PhC parameters such as lattice constant, hole diameter, or etching depths of the air holes do not need to be stringently controlled [20], [34]. The large tolerances in the fabrication process make PhC VCSELs suitable for mass production and thus an excellent candidate for low-cost/high-volume consumer applications.

In this paper, we investigate the optical properties of proton-implanted red PhC VCSELs and examine the dependence of the output beam divergence on different etching depth of the PhC air holes. The fabricated proton-implanted red PhC VCSELs show a single-fundamental-mode output power greater than 1 mW at room temperature. The emission wavelength of the PhC VCSELs at room temperature is 674 nm. As a result of the weak step-index guidance profile introduced by the PhC, the lasers possess a circular Gaussian-like far-field pattern with a stable beam divergence angle that is independent of injection current or ambient temperature. Red PhC VCSELs can either be optimized for low beam divergence or low threshold currents depending on the etching depth chosen for the PhC air holes.

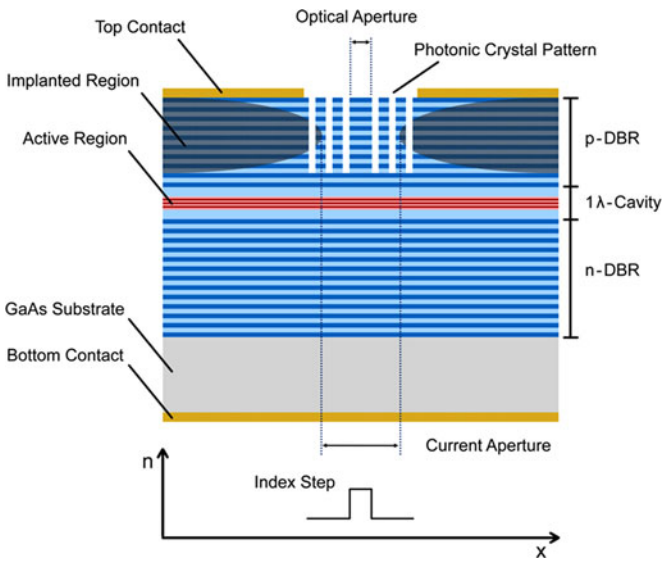

Fig. 1. Cross-sectional schematic of a proton-implanted PhC VCSEL.

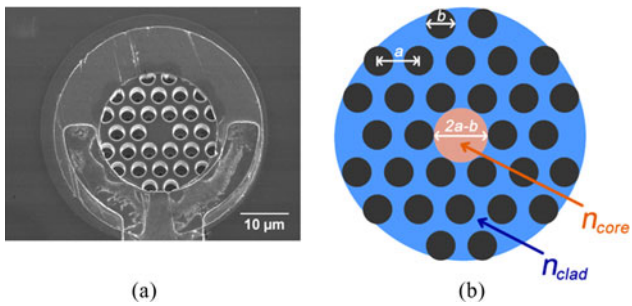

Fig. 2. (a) Top view image of a fabricated PhC VCSEL and (b) PhC pattern with parameters labeled.

II. PhC VCSEL Design

The epitaxial structure used for the fabrication of the proton-implanted red PhC VCSELs is grown by metal-organic chemical vapor deposition on an n-GaAs substrate. The diode laser structure is comprised of a top p-type distributed Bragg reflector (DBR) mirror, an active region, and a bottom n-type DBR mirror. The DBR periods are composed of high-index $Al_{0.5}Ga_{0.5}As$ and low-index $Al_{0.92}Ga_{0.08}As$ quarter-wave layers. The intrinsic 1–λ optical cavity contains InGaP quantum wells.

Fig. 1 shows a cross-sectional schematic of a fabricated proton-implanted red PhC VCSEL. We start the fabrication process with the deposition of top p-type metal (Ti/Au) and bottom n-type metal (AuGe/Ni/Au) contacts. Proton-implant apertures with the diameters of 10 and 12 μm are defined by ion implantation to serve as current confinement. Next, PhC patterns are transferred using optical lithography into the top facet of the VCSELs and etched using inductively coupled plasma reactive ion etching. The PhC patterns consist of a periodic hexagonal array of circular air holes. A center defect creates a transverse index-confinement structure that serves as optical confinement. Design parameters for the PhC patterns are: lattice constant a, hole diameter b, resulting center defect diameter $2a-b$, and the etching depth of the PhC air holes. Scanning electron micrograph of a fabricated red PhC VCSEL and sketch of the corresponding PhC pattern are depicted in Fig. 2. The defect diameter, lattice constant, and hole diameter of the PhC patterns studied here are 5.6, 4, and 2.4 μm for the 10-μm implant aperture VCSEL, and 5.85, 4.5, and 3.15 μm for the 12-μm implant aperture VCSEL, respectively. The proton-implanted aperture, serving as electrical confinement, is chosen to be larger than the PhC defect region to guarantee that the index profile induced by the thermal lens follows a uniform distribution across the PhC defect region. The refractive index contrast of the thermal lens arising under continuous wave operation is on the order of 5×10^{-3} whereas the magnitude of the PhC step-index ranges from 5×10^{-4} to 5×10^{-3} for etching depths of 70–100% into the top DBR, respectively. The combination of index guiding in the center defect region and induced loss for higher order modes in

the PhC region results in single-fundamental-mode operation. The effects of loss on modal discrimination are discussed in more detail elsewhere [35], [36].

III. PhC VCSEL Modeling

A step-index waveguide can be used to describe PhC VCSELs with a single center defect, as described previously [17]–[20]. In this model, the center defect of the PhC is taken as the core of the optical waveguide, and the surrounding PhC region with its reduced refractive index is taken as a cladding region. This approach has the advantage of being computationally less intensive than other more rigorous methods such as finite-difference time domain, finite element, or 3-D calculations [37]–[39] and serves the purpose of helping with the design of single-mode PhC VCSELs. By using the plane-wave expansion method, the real part of the effective refractive index of the cladding region can be found by calculating the band diagram of the PhC in each DBR layer that is penetrated by air holes. In this procedure, the effective refractive index is determined by taking the inverse of the slope of the out-of-plane propagation. This effective refractive index can then be used to replace the DBR layers penetrated with PhC air holes by homogeneous effective index layers [18]. The effective index VCSEL structure can then be used to calculate the resonances of the core and the cladding region using a 1-D transmission matrix approach. The difference in resonance wavelengths is directly proportional to the step-index difference between the center core and the PhC cladding region and is described by [40]

$$\frac{\Delta n_{\text{eff}}}{n_{\text{eff}}} \approx \frac{\Delta \lambda_o}{\lambda_o} \tag{1}$$

where n_{eff} and Δn_{eff} are the effective refractive index of the core and the effective index difference between the core and the cladding region, respectively, and λ_o and $\Delta\lambda_o$ are the free-space core resonance wavelength and the resonance wavelength difference between the core and the cladding region, respectively. By using this approach, the finite etching depth of PhC air holes in the top DBR is intrinsically accounted for. A field-weighted average of the DBR center region is used to determine the core refractive index n_{core} in the waveguide model. The waveguide cladding index n_{clad} is found by taking the difference between the core index n_{core} and the effective refractive index difference Δn_{eff}. The mode cutoff for the single-mode emission of the PhC VCSEL can be determined by the normalized frequency parameter V_{eff}, which is defined by [41]

$$V_{\text{eff}} \approx \frac{\pi D}{\lambda_o}\sqrt{n_{\text{core}}^2 - n_{\text{clad}}^2} \tag{2}$$

where D is the PhC defect diameter, λ_o is the free-space lasing wavelength, and n_{core} and n_{clad} are the refractive indices in the core and the cladding region, respectively. The single-mode condition is found to be [41]

$$V_{\text{eff}} < 2.405. \tag{3}$$

Fig. 3 shows the procedure used to calculate the step-index waveguide model. We can further compute the near-field mode profile of the PhC VCSEL and by using its Fourier transform,

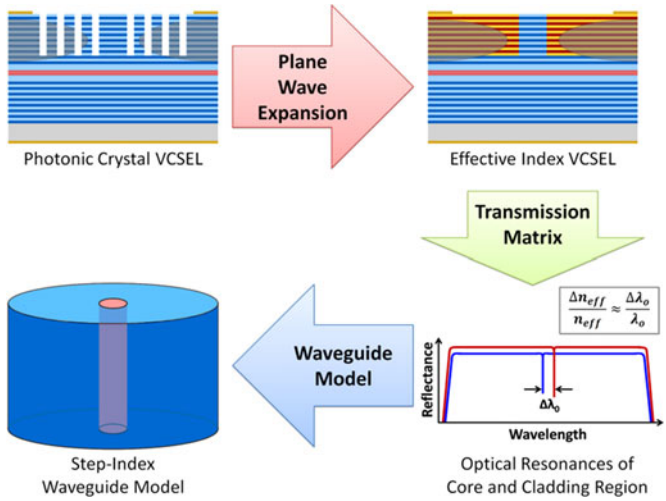

Fig. 3. Procedure used to calculate the effective refractive index of the PhC cladding region to design the step-index waveguide model.

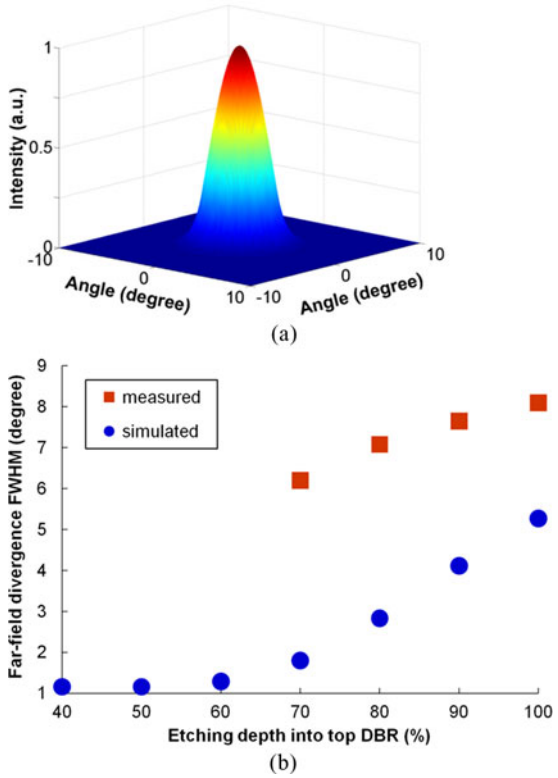

Fig. 4. Far-field beam divergence of a 680-nm PhC VCSEL. (a) Simulated far-field profile for 100% etching depth into the top DBR. (b) Simulated and measured far-field beam divergence for different etching depths. For shallow etched PhC holes (etching depth $< 70\%$), the optical loss becomes so large that the PhC VCSELs do not lase.

we can calculate the far-field mode profile as a function of PhC design and etching depth. Fig. 4(a) shows the far-field beam divergence of a 680-nm PhC VCSEL with $b/a = 0.7$, $a = 4.5\,\mu$m, and 90% etching depth into the top DBR. The experimental and theoretically calculated far-field beam divergences for different etching depths are shown in Fig. 4(b). The experimental measurement of the contribution of scattering loss and

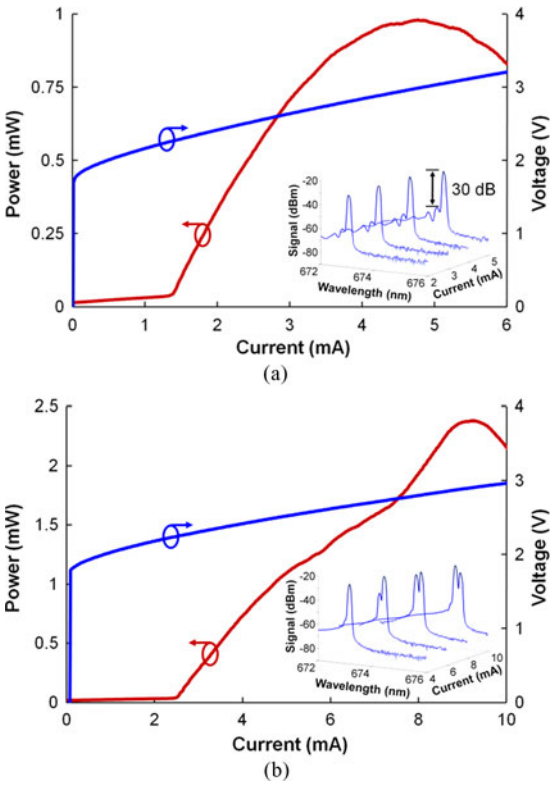

Fig. 5. Light output and applied voltage with spectral characteristics for red proton-implanted VCSELs. (a) A PhC VCSEL with $b/a = 0.7$, $a = 4.5\,\mu$m, and 90% etching depth into the top DBR. (b) Unetched control device.

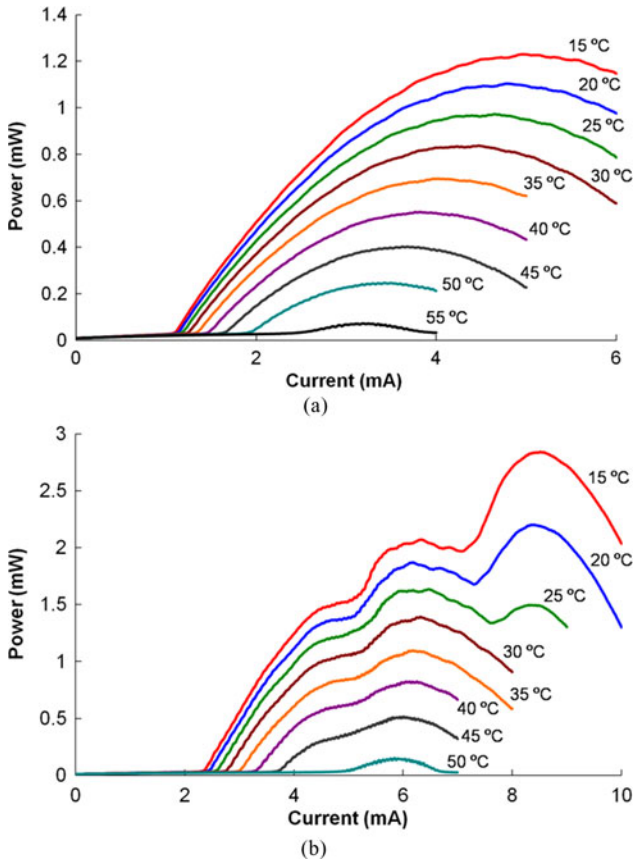

Fig. 6. Light output current characteristics for various ambient temperatures. (a) A red PhC VCSEL with $b/a = 0.7$, $a = 4.5\,\mu$m, and 90% etching depth into the top DBR. (b) Unetched control device.

thermally induced index changes in Fig. 4 proved elusive. From our simulations, for shallow PhC etches, the scattering loss will dominate [36], while for deeper etches, the thermally induced index shift will become stronger due to the greater removal of the semiconductor material. For etching depths deeper than 60% into the top DBR, the index-confinement induced by the PhC holes produces a significant confinement of the electrical near-field, which results in an increase in far-field beam divergence. The step-index waveguide model used here only considers confinement due to index contrast, whereas sources of confinement such as optical scattering loss [35], [36] or thermally induced index confinement are neglected. Thus, the simulated beam-divergence values are lower bounds for the experimentally observed data shown in Fig. 4.

IV. Experimental Results

The light versus current and voltage characteristics with corresponding optical spectra for the 12-μm implant aperture VCSELs are depicted in Fig. 5. The PhC VCSEL operates in a single fundamental mode from threshold through maximum output power with a side-mode suppression ratio greater than 30 dB. The single-mode output power of the PhC VCSEL is found to be greater than 1 mW at room temperature. Due to the step-index optical confinement provided by the PhC, the lasing threshold is 1.3 mA. In comparison, the control VCSEL without a PhC has a multimode operation to a maximum output power of greater than 2 mW, and a higher threshold current of 2.4 mA, due to the thermally induced optical confinement needed for lasing. The electrical characteristics of the PhC VCSEL remains virtually unchanged compared to the unetched control device. Previous studies have shown that there is no negative impact on the reliability of PhC VCSELs due to the etched air holes into the top facet [34].

We also investigate the thermal characteristics of the fabricated VCSELs. Fig. 6 shows the LI curves of a 680-nm PhC VCSEL ($b/a = 0.7$, $a = 4.5\,\mu$m, 90% etching depth into top DBR, and implant aperture $= 12\,\mu$m) and unetched control laser for different ambient temperatures. The PhC VCSEL shows lasing action for temperatures up to 55 °C. As one would expect, the maximum output power decreases with increasing surrounding temperatures. The maximum continuous wave (CW) lasing temperature of 55 °C is a typical value for red VCSELs emitting at wavelengths around 680 nm since high temperature performance is limited by the relatively small conduction band offset of the InGaP active material system leading to high leakage current.

The far-field dependence of red PhC VCSELs is investigated in more detail by comparing a PhC VCSEL ($b/a = 0.7$, $a = 4.5\,\mu$m, 90% etching depth into top DBR, and implant aperture $= 12\,\mu$m) with a corresponding control device. Fig. 7(a) shows the full-width half-maximum (FWHM) far-field beam divergence of the PhC VCSEL and the corresponding unetched

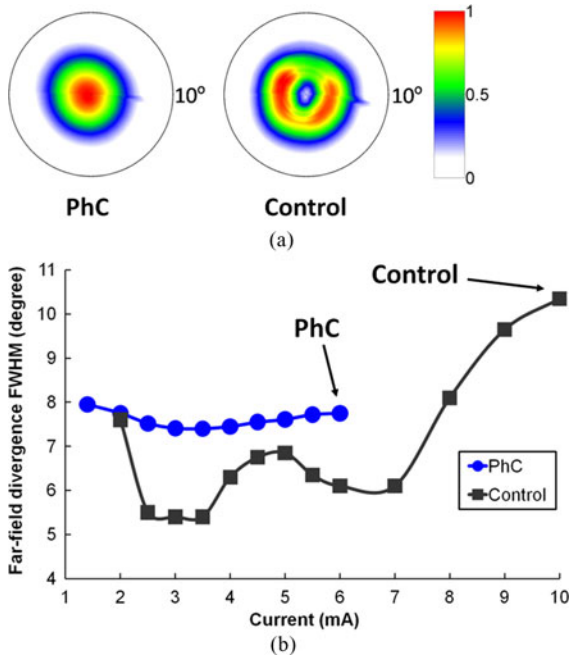

Fig. 7. Far-field dependence of a PhC VCSEL and proton-implanted control laser. (a) Top-view intensity profile at maximum injection current. (b) FWHM of far-field divergence angle for varying injection current.

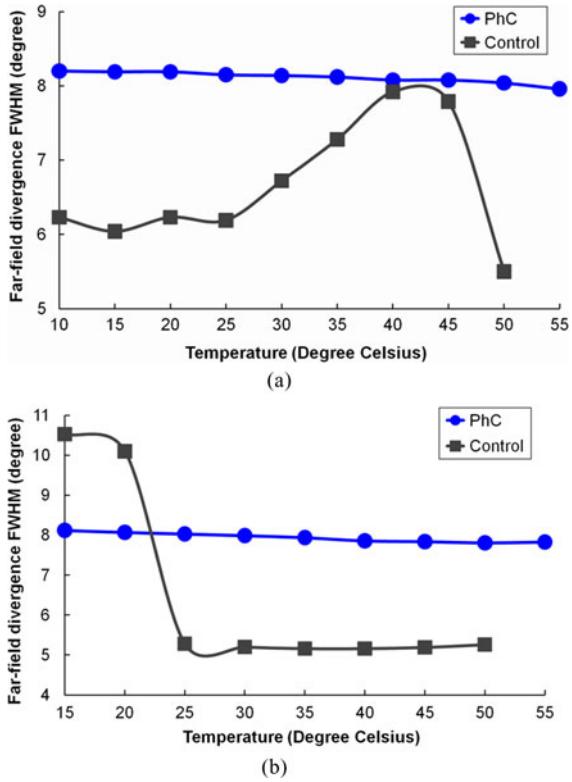

Fig. 8. Far-field divergence angle of a PhC VCSEL and corresponding control laser for varying ambient temperatures. (a) Injection current level at $1.1 \times I_{\mathrm{th}}$. (b) Injection current level at maximum output power.

control VCSEL for various levels of current injection. Due to the step-index induced by the PhC, stable optical confinement for all levels of current injection is observed. As a result, the far-field beam divergence of the PhC VCSEL does not change significantly with injection current. The far-field beam divergence is inversely proportional to the near-field mode size that is determined by the PhC defect diameter and etching depth of the PhC air holes. This is in contrast to the far-field beam divergence of the proton-implanted control VCSEL that shows a strong dependence on current injection, as can be seen in Fig. 7. For low levels of current near threshold, the control VCSEL has a divergence angle similar to the PhC VCSEL. With increasing current, the control device operates single mode with a small divergence angle due to the influence of the thermal lens. The narrow divergence arises from the fact that the thermal lens extends over the entire implant aperture that is larger than the PhC defect. For higher levels of current injection, the control implant VCSEL becomes multimode and the far-field beam divergence increases. In addition to the fluctuations in beam divergence, it is observed that the far-field beam profile of the control device does not resemble a Gaussian mode shape. Moreover, random beam steering of the intensity maxima due to local fluctuations of the thermal lens can also be observed. The index-step provided by the PhC can be engineered to be similar in magnitude to the thermally induced index profile, but remains constant to avoid beam fluctuations.

We also investigate the dependence of the far-field beam divergence for varying ambient temperatures by comparing the red PhC VCSEL ($b/a = 0.6$, $a = 4\,\mu$m, 80% etching depth into top DBR, and implant aperture $= 10\,\mu$m) with a corresponding control device. In Fig. 8(a), the level of current injection is held constant at $1.1 \times I_{\mathrm{th}}$, whereas the surrounding temperature is varied from 15 to 55 °C in steps of 5 °C. Fig. 8(b) shows that the far-field beam divergence for varying temperatures at injection current levels at maximum output power. The PhC VCSEL shows a stable far-field beam divergence under both conditions of low and high levels of current injection, over the entire temperature range. This is in contrast to large changes in far-field beam divergence observed for the unetched control laser. The control implant VCSEL has a low and stable beam divergence for elevated temperatures when operated close to maximum output power due to the fact that the higher order modes of the control device apparently do not overcome lasing threshold at higher temperatures.

V. Analysis and Discussion

The incorporation of a PhC into the top facet of a proton-implanted VCSEL stabilizes the optical output beam. A stable optical beam profile for different levels of injection current and various ambient temperatures is desirable for VCSELs emitting in the visible spectrum due to many applications that demand high-quality optical beam properties. The beam properties of PhC VCSELs can be controlled by the design of the PhC pattern as well as by the etching depth of the PhC air holes. Previous works have shown that the requirements on the hole pattern for single-mode operation in PhC VCSELs are not stringent [20], [34]. However, there is a strong dependence of electrical and optical characteristics on the etching depth of the PhC air holes.

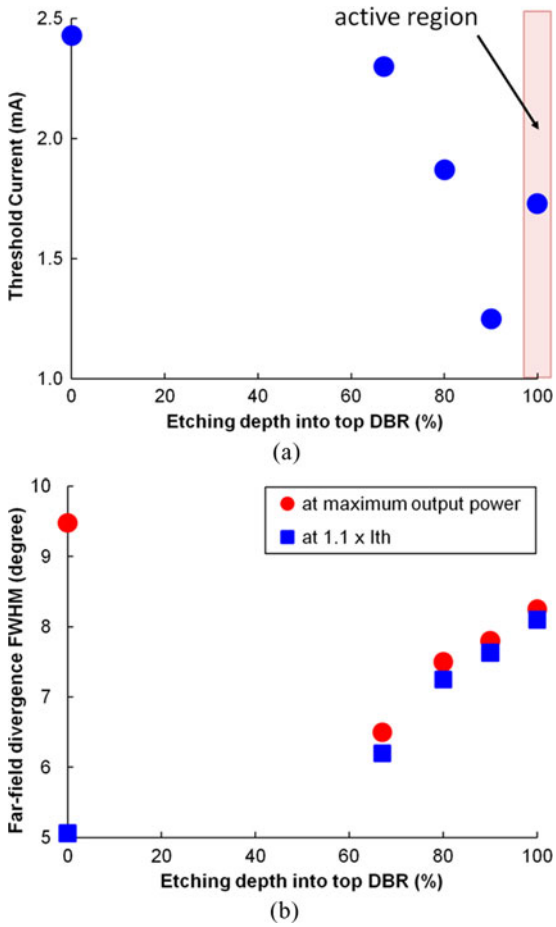

Fig. 9. Etching depth dependence of a red PhC VCSEL. (a) Threshold current. (b) Far-field beam divergence.

The impact of etching depth on PhC VCSEL characteristics such as threshold current and far-field beam divergence is shown in Fig. 9 for a red PhC VCSEL with the hole to lattice spacing ratio $b/a = 0.7$, lattice spacing $a = 4.5\,\mu$m, and implant aperture $= 12\,\mu$m. Fig. 9(a) displays the threshold current dependence on different PhC etching depths ranging from 0% to 100% into the top DBR. An etching depth of 100% corresponds to PhC holes etched all the way through the top DBR into the active region. A minimum in threshold current is observed for etching depths close to but not through the active region. High threshold currents are observed for shallow PhC etches as a result of high scattering loss as well as for holes etched through the active region. The nonradiative recombination of electron–hole pairs on the PhC hole sidewalls in the quantum wells results in an increase in loss and increase in threshold current. The optimal etching depth for the PhC holes, in terms of threshold current, is close to but not into the active region, as can be seen from Fig. 9(a). The etching depth of the PhC holes can also influence the beam properties of PhC VCSELs as shown in Fig. 9(b). The round data points show the divergence angle when operated at maximum output power and the square data points show the divergence when operated at $1.1 \times I_{\rm th}$. It is noteworthy that the beam of the PhC VCSEL is constant for changes in injection current. By contrast, the unetched control VCSEL (0% etching depth) in Fig. 9(b) shows a wide variation of divergence angle with varying injection current. The change in the far-field divergence angle for the control VCSEL was found to be more than 4.5° (full angle). As described previously, the PhC helps to stabilize the output beam so that changes in far-field beam divergence for different levels of current injection are minimal, as can be seen in Fig. 9(b). With the increasing etching depth, the beam divergence discrepancy between the high and the low levels of current injection becomes smaller. Furthermore, it can be observed that the beam divergence of the red PhC VCSEL increases with increasing etching depth. This is due to the fact that deeper PhC etches result in a larger index step and therefore provide higher optical confinement for the near-field, resulting in an increase in the far-field divergence angle. This phenomenon has previously been reported for 850-nm oxide PhC VCSELs [42].

VI. Summary

In summary, we have fabricated and characterized the electrical and optical properties of proton-implanted PhC VCSELs emitting in the visible spectrum. The PhC VCSELs, emitting at a wavelength of 674 nm, demonstrate stable-single-mode beam properties. The PhC air holes etched in the top facet of the VCSELs serve as a weakly index-guided structure and allow for a stable low-divergence output beam with an FWHM as low as 6°. A single-fundamental-mode operation with a side-mode suppression ratio larger than 30 dB and a stable Gaussian-like far-field profile for all levels of current injection and various ambient temperatures have been observed. The maximum achievable CW lasing temperature of the PhC VCSELs is found to be 55 °C. By varying the design and etching depth of the PhC pattern, the PhC VCSELs can either be optimized for low beam divergence or low threshold current. In order to optimize the electrical characteristics of PhC VCSELs, deeper PhC etches close to the active region are desirable. For a narrow optical output beam, shallower etches resulting in a low index step and, therefore, low far-field beam divergence can be achieved.

References

[1] A. M. Kasten, A. V. Giannopoulos, C. Long, C. Chen, and K. D. Choquette, "Fabrication and characterization of individually addressable vertical-cavity surface-emitting laser arrays and integrated VCSEL/PIN detector arrays," *Proc. SPIE*, vol. 6484, p. 64840 C, 2007.

[2] J.-S. Pan, Y.-S. Lin, C.-F. Li, H.-C. Lai, C.-C. Wu, and K.-F. Huang, "850 nm implanted and oxide VCSELs in multi-gigabit data communication application," *Proc. SPIE–Optoelectron., Mater., Devices Commun.*, vol. 4580, pp. 46–51, 2001.

[3] F. Koyama, S. Shinada, K. Goto, and K. Iga, "Surface emitting lasers for optical near-field data storage," *Proc. SPIE*, vol. 3899, pp. 344–350, 1999.

[4] M. K. Hibbs-Brenner, K. L. Johnson, and M. Bendett, "VCSEL technology for medical diagnostics and therapeutics," *Proc. SPIE*, vol. 7180, p. 71800 T, 2009.

[5] K. Keränen, T. Saastamoinen, J.-T. Mäkinen, M. Silvennoinen, I. Mustonen, P. Vahimaa, T. Jääskeläinen, A. Lento, A. Ojapalo, M. Schorpp, P. Hoskio, and P. Karioja, "Injection moulding integration of a red VCSEL illuminator module for a hologram reader sensor," *Proc. SPIE*, vol. 6585, p. 658503, 2007.

[6] S.-W. Chiou, Y.-C. Lee, C.-S. Chang, and T.-P. Chen, "High speed red RCLEDs and VCSELs for plastic optical fiber application," *Proc. SPIE*, vol. 5735, pp. 129–133, 2005.

[7] J. D. Lambkin, T. Calvert, B. Corbett, J. Woodhead, S. M. Pinches, A. Onischenko, T. E. Sale, J. Hosea, P. V. Daele, K. Vandeputte, A. V. Hove, A. Valster, J. G. McInerney, and P. A. Porta, "Development of a red VCSEL-to-plastic fiber module for use in parallel optical data links," *Proc. SPIE*, vol. 3946, pp. 95–105, 2000.

[8] F. Mederer, R. Jäger, P. Schnitzer, H. Unold, M. Kicherer, K. J. Ebeling, M. Naritomi, and R. Yoshida, "Multi-gigabit/s perfluorinated graded-index plastic-optical-fiber data links with butt-coupled single-mode InGaAs VCSEL," *Proc. SPIE*, vol. 3896, pp. 273–280, 1999.

[9] C. Jung, R. Jager, M. Grabherr, P. Schnitzer, R. Michalzik, B. Weigl, S. Muller, and K. J. Ebeling, "4.8 mW single-mode oxide confined top surface emitting vertical-cavity laser diodes," *Electron. Lett.*, vol. 33, no. 21, pp. 1790–1791, 1997.

[10] R. A. Morgan, G. D. Guth, M. W. Focht, M. T. Asom, K. Kojima, L. E. Rogers, and S. E. Callis, "Transverse mode control of vertical cavity top-surface-emitting lasers," *IEEE Photon. Technol. Lett.*, vol. 5, no. 4, pp. 374–377, Apr. 1993.

[11] E. W. Young, K. D. Choquette, S. L. Chuang, K. M. Geib, A. J. Fischer, and A. A. Allerman, "Single-transverse-mode vertical-cavity lasers under continuous and pulsed operation," *IEEE Photon. Technol. Lett.*, vol. 13, no. 9, pp. 927–929, Sep. 2001.

[12] H. Martinsson, J. A. Vukusic, M. Grabherr, R. Michalzik, R. Jager, K. J. Ebeling, and A. Larsson, "Transverse mode selection in large-area oxide-confined vertical-cavity surface-emitting lasers using a shallow surface relief," *IEEE Photon. Technol. Lett.*, vol. 11, no. 12, pp. 1536–1538, Dec. 1999.

[13] H. J. Unold, S. W. Z. Mahmoud, R. Jager, M. Kicherer, M. C. Riedl, and K. J. Ebeling, "Improving single-mode VCSEL performance by introducing a long monolithic cavity," *IEEE Photon. Technol. Lett.*, vol. 12, no. 8, pp. 939–941, Aug. 2000.

[14] A. Furukawa, S. Sasaki, M. Hoshi, A. Matsuzono, K. Moritoh, and T. Baba, "High-power single-mode vertical-cavity surface-emitting lasers with triangular holey structure," *Appl. Phys. Lett.*, vol. 85, pp. 5161–5163, 2004.

[15] P. O. Leisher, A. J. Danner, J. J. Raftery, Jr., and K. D. Choquette, "Proton implanted single mode holey vertical-cavity surface emitting lasers," *Electron. Lett.*, vol. 41, no. 18, pp. 1010–1011, 2005.

[16] D. S. Song, S. H. Kim, H. G. Park, C. K. Kim, and Y. H. Lee, "Single-fundamental-mode photonic-crystal vertical-cavity surface- emitting lasers," *Appl. Phys. Lett.*, vol. 80, pp. 3901–3903, 2002.

[17] N. Yokouchi, A. J. Danner, and K. D. Choquette, "Two-dimensional photonic crystal confined vertical-cavity surface-emitting lasers," *IEEE J. Sel. Topics Quantum Electron.*, vol. 9, no. 5, pp. 1439–1445, Sep./Oct. 2003.

[18] A. J. Danner, J. J. Raftery, Jr., T. Kim, P. O. Leisher, A. V. Giannopoulos, and K. D. Choquette, "Progress in photonic crystal vertical cavity lasers," *IEICE Trans. Electron.*, vol. E88-C, no. 5, pp. 944–950, 2005.

[19] N. Yokouchi, A. J. Danner, and K. D. Choquette, "Etching depth dependence of the effective refractive index in two-dimensional photonic crystal-patterned vertical-cavity surface-emitting laser structures," *Appl. Phys. Lett.*, vol. 82, no. 9, pp. 1344–1346, 2003.

[20] A. J. Danner, T. S. Kim, and K. D. Choquette, "Single fundamental mode photonic crystal vertical cavity laser with improved output power," *Electron. Lett.*, vol. 41, no. 6, pp. 325–326, 2005.

[21] H. P. D. Yang, F. I. Lai, Y. H. Chang, H. C. Yu, C. P. Sung, H. C. Kuo, S. C. Wang, S. Y. Lin, and J. Y. Chi, "Single-mode (SMSR $>$ 40 dB) proton-implanted photonic crystal vertical-cavity surface emitting lasers," *Electron. Lett.*, vol. 41, no. 6, pp. 326–328, 2005.

[22] A. M. Kasten, M. P. Tan, J. D. Sulkin, P. O. Leisher, and K. D. Choquette, "Photonic crystal vertical cavity lasers with wavelength-independent single-mode behavior," *Photon. Tech. Lett.*, vol. 20, pp. 2010–2012, 2008.

[23] K. D. Choquette, R. P. Schneider, M. Hagerott Crawford, K. M. Geib, and J. J. Figiel, "Continuous wave operation of nm selective oxidized AlGaInP vertical-cavity lasers," *Electron. Lett.*, vol. 31, pp. 640–660, 1995.

[24] R. P. Schneider, Jr., K. D. Choquette, J. A. Lott, K. L. Lear, J. J. Figiel, and K. J. Malloy, "Efficient room-temperature continuous-wave AlGaInP/AlGaAs visible (670 nm) vertical-cavity surface-emitting laser diodes," *IEEE Photon. Technol. Lett.*, vol. 6, no. 3, pp. 313–316, Mar. 1994.

[25] M. H. Crawford, R. P. Schneider, Jr., K. D. Choquette, and K. L. Lear, "Temperature-dependent characteristics and single-mode performance of AlGaInP-based 670–690-nm vertical-cavity surface-emitting lasers," *IEEE Photon. Technol. Lett.*, vol. 7, no. 7, pp. 724–726, Jul. 1995.

[26] J. A. Lehman, R. A. Morgan, D. Carlson, M. Hagerott Crawford, and K. D. Choquette, "High-frequency modulation characteristics of red VCSELs," *Electron. Lett.*, vol. 33, pp. 298–300, 1996.

[27] W. W. Chow, K. D. Choquette, M. H. Crawford, K. L. Lear, and G. R. Hadley, "Design, fabrication, and performance of infrared and visible vertical-cavity surface-emitting lasers," *IEEE J. Quantum Electron.*, vol. 33, no. 10, pp. 1810–1824, Oct. 1997.

[28] K. Takaoka, M. Ishikawa, and G.-I. Hatakoshi, "Low-threshold and high-temperature operation of InGaAlP-based proton-implanted red VCSELs," *IEEE J. Sel. Topics Quantum Electron.*, vol. 7, no. 2, pp. 381–385, Mar./Apr. 2001.

[29] M. Grabherr, M. Miller, R. Jäger, R. Michalzik, U. Martin, H. J. Unold, and K. J. Ebeling, "High-power VCSELs: Single devices and densely packed 2-D-arrays," *IEEE J. Sel. Topics Quantum Electron.*, vol. 5, no. 3, pp. 495–502, May/Jun. 1999.

[30] G. M. Yang, M. H. MacDougal, and P. D. Dapkus, "Ultralow threshold current vertical-cavity surface-emitting lasers obtained with selective oxidation," *Electron. Lett.*, vol. 31, pp. 886–888, 1995.

[31] R. Jäger, M. Grabherr,C. Jung, R. Michalzik, G. Reiner, B. Weigl, and K. J. Ebeling, "57% wallplug efficiency oxide-confined 850 nm wavelength GaAs VCSELs," *Electron. Lett.*, vol. 33, pp. 330–331, 1997.

[32] B. Weigl, M. Grabherr, R. Michalzik, G. Reiner, and K. J. Ebeling, "High power single-mode selectively oxidized vertical-cavity surface emitting lasers," *IEEE Photon. Technol. Lett.*, vol. 8, no. 8, pp. 971–973, Aug. 1996.

[33] P. O. Leisher, J. D. Sulkin, and K. D. Choquette, "Parametric study of proton implanted photonic crystal vertical cavity surface emitting lasers," *IEEE J. Sel. Topics Quantum Electron.*, vol. 13, no. 5, pp. 1290–1294, Sep./Oct. 2007.

[34] A. M. Kasten, J. D. Sulkin, P. O. Leisher, D. K. Mc Elfresh, D. Vacar, and K. D. Choquette, "Manufacturable photonic crystal single mode and fluidic vertical cavity surface emitting lasers," *IEEE J. Sel. Topics Quantum Electron.*, vol. 14, no. 4, pp. 1123–1131, Jul./Aug. 2008.

[35] D. F. Siriani, M. P. Tan, A. M. Kasten, A. C. Lehman Harren, P. O. Leisher, J. D. Sulkin, J. J. Raftery, A. J. Danner, A. V. Giannopoulos, and K. D. Choquette, "Mode control in photonic crystal vertical-cavity surface-emitting lasers and coherent arrays," *IEEE J. Sel. Topics Quantum Electron.*, vol. 15, no. 3, pp. 909–917, May/Jun. 2009.

[36] D. F. Siriani, P. O. Leisher, and K. D. Choquette, "Loss-induced confinement in photonic crystal vertical-cavity surface-emitting lasers," *IEEE J. Quantum Electron.*, vol. 45, no. 7, pp. 762–768, Jul. 2009.

[37] P. Bienstman, R. Baets, J. Vukusic, A. Larsson, M. J. Noble, M. Brunner, K. Gulden, P. Debernardi, L. Fratta, G. P. Bava, H. Wenzel, B. Klein, O. Conradi, R. Pregla, S. A. Riyopoulos, J.-F. P. Seurin, and S. L. Chuang, "Comparison of optical VCSEL models on the simulation of oxide-confined devices," *IEEE J. Quantum Electron.*, vol. 37, no. 12, pp. 1618–1631, Dec. 2001.

[38] T. Czyszanowski, M. Dems, and K. Panajotov, "Singlemode condition and modes discrimination in photonic-crystal 1.3 μm AlInGaAs/InPVCSEL," *Opt. Exp.*, vol. 15, no. 9, pp. 5604–5608, 2007.

[39] T. Czyszanowski, M. Dems, and K. Panajotov, "Optimal parameters of photonic crystal vertical-cavity surface-emitting diode lasers," *IEEE J. Lightw. Technol.*, vol. 25, no. 9, pp. 2331–2336, Sep. 2007.

[40] G. R. Hadley, "Effective index model for vertical-cavity surface emitting lasers," *Opt. Lett.*, vol. 20, no. 13, pp. 1483–1485, 1995.

[41] B. E. A. Saleh and M. C. Teich, *Fundamentals of Photonics*. New York: Wiley, 1991.

[42] A. Liu, M. Xing, H. Qu, W. Chen, W. Zhou, and W. Zheng, "Reduced divergence angle of photonic crystal vertical-cavity surface-emitting laser," *Appl. Phys. Lett.*, vol. 94, pp. 191105-1–191105-3, 2009.

Ansas M. Kasten (S'07) was born in Saarbrücken, Germany, on June 9, 1977. He received the Dipl.-Ing. in electrical engineering from the University of Saarland, Saarbrücken, Germany, in 2003, and the M.S. and Ph.D. degrees in electrical and computer engineering from the University of Illinois at Urbana-Champaign, Urbana, IL, in 2006 and 2010, respectively, where he is currently holding a Postdoctoral Research appointment.

From 2003 to 2004, he was a visiting scholar in the Department of Agricultural and Biological Engineering, University of Illinois, where he later joined the Photonic Device Research Group. His current research interests include vertical-cavity surface-emitting lasers (VCSELs), photonic crystal VCSELs, high-power VCSEL arrays, low-noise photodetectors, and optofluidic microchips.

Mr. Kasten is a Student Member of the IEEE Photonics Society and the Optical Society of America.

Dominic F. Siriani (S'07) received the B.S. and M.S. degrees in electrical engineering from the University of Illinois at Urbana-Champaign, Urbana, IL, in 2006 and 2007, respectively, where he is currently working toward the Ph.D. degree in electrical engineering.

His research interests include photonic crystal vertical-cavity surface-emitting lasers (VCSELs), VCSEL arrays, beam combining and beam steering, coupled mode theory, and coherence theory.

Mr. Siriani is a Student Member of IEEE/Photonics Society, a National Science Foundation (NSF) Graduate Fellow, and a National Defense Science and Engineering Graduate (NDSEG) Fellow.

Mary K. Hibbs-Brenner (M'88) received the B.A. degree in physics from Carleton College, Northfield, MN, in 1977, and the Ph.D. degree in materials science from Stanford University, Stanford CA, in 1982, and the MBA degree from the Carlson School of Business, University of Minnesota, Minneapolis, in 2004.

She was a Postdoctoral Researcher at the University of Linköping, Linköping, Sweden, for two years. She is a Cofounder and Chief Executive Officer of Vixar since 2005, which offers unique vertical-cavity surface-emitting laser (VCSEL) components to the industrial, medical, consumer, and office equipment markets. Prior to cofounding Vixar, she held business development, technical management, and research positions at Honeywell. She was responsible for initiating and developing the company's VCSEL business, which offered VCSEL products for fiber optic links within local area networks and storage area networks. She also served as a business development lead within the Honeywell Technology organization, developing business plans for bringing new technologies to market. She has seven patents, and more than 50 publications and invited presentations.

Klein L. Johnson received the B.A. degree in mathematics and physics from St. Olaf College, Northfield, MN, and the Ph.D. degree in electrical engineering from the University of Minnesota, Minneapolis.

He is a Cofounder of Vixar and its Chief Technology Officer since 2005. Prior to cofounding Vixar, he spent 12 years at Honeywell as a Research Scientist and Project Leader. His work spanned a broad range of research and development in optoelectronic device and packaging, including the development of polymer and glass waveguides, a very high bandwidth array transceiver, optoelectronic integrated circuits, and rugged packaging for military applications. He has three patents, seven patent applications, and is the author/coauthor of multiple papers and conference presentations.

Kent D. Choquette (M'97–F'03) received the dual B.S. degrees in engineering physics and applied mathematics from the University of Colorado-Boulder, Boulder, in 1984 and the M.S. and Ph.D. degrees in materials science from the University of Wisconsin-Madison, Madison, in 1985 and 1990, respectively.

From 1990 to 1992, he held a Postdoctoral appointment at AT&T Bell Laboratories, Murray Hill, NJ. He joined Sandia National Laboratories in Albuquerque, NM from 1993 to 2000. He became a Professor in the Department of Electrical and Computer Engineering, University of Illinois, Urbana, in 2000. His Photonic Device Research Group pursues the design, fabrication, characterization, and applications of vertical cavity surface-emitting lasers (VCSELs), photonic crystal light sources, nanofabrication technologies, and hybrid integration techniques for photonic devices. He has authored more than 200 technical publications and three book chapters, and has presented numerous invited talks and tutorials.

Dr. Choquette served as an Associate Editor of the *IEEE Journal of Quantum Electronics*, *IEEE Photonic Technology Letters*, and *J. Lightwave Technology*, as well as a Guest Editor of *IEEE Journal of Selected Topics in Quantum Electronics*. He was awarded the 2008 IEEE/LEOS Engineering Achievement Award. He is a Fellow of the Optical Society of America and SPIE.